Complete mapping of energy transfer pathways in the plant light-harvesting complex Lhca4

Martijn Tros[a*], Vladimir I. Novoderezhkin[b], Roberta Croce[a], Rienk van Grondelle[a], Elisabet Romero[c]

[a]Department of Biophysics, Faculty of Sciences, VU University Amsterdam and LaserLaB Amsterdam, De Boelelaan 1081, 1081 HV Amsterdam, the Netherlands

[b]A. N. Belozersky Institute of Physico-Chemical Biology, Moscow State University, Leninskie Gory, 119992 Moscow, Russia

[c]Institute of Chemical Research of Catalonia (ICIQ), Barcelona Institute of Science and Technology (BIST), Avinguda dels Països Catalans 16, 43007 Tarragona, Spain

*Martijn Tros, m.tros@vu.nl

Supplementary Information

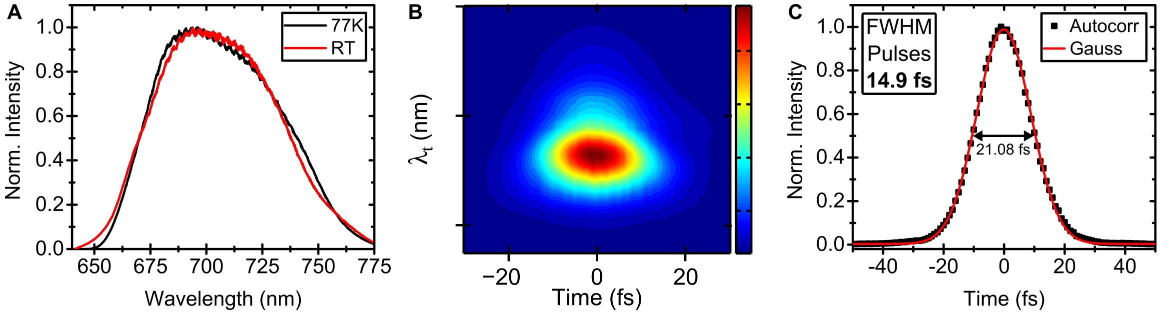

Figure S1. Ultrafast pulses used in the 2DES experiments. A) Spectral shape of the used pulses in the 77 K (black) and RT (red) measurements. The intensity is normalized to the maximum (at 695 nm). B) Profile of the frequency resolved optical gating (FROG) of the second harmonic (SH) pulse of the beams 1 and 2. C) Horizontal trace of the SH-FROG profile showing the autocorrelation signal (black). By means of a Gaussian fit (red line) the FWHM of the autocorrelation was determined. The corresponding FWHM of the 2DES pulses: 21.08/√2 = 14.9 fs.

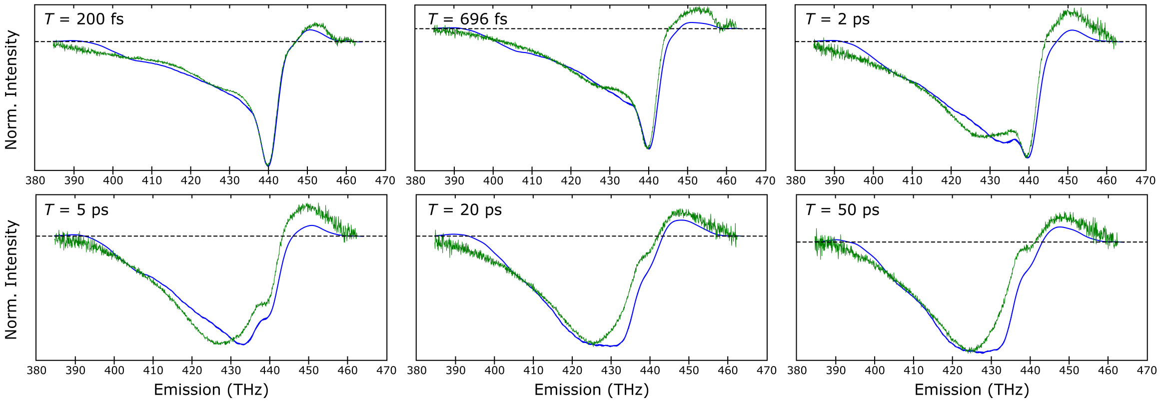

Figure S2. Phasing of the 2DES data of WT Lhca4 at 77K. The phase is retrieved by means of the projection slice theorem, in which the projection of the real signal of the 2DES spectrum (blue) is compared to the measured pump-probe data (green).[1] The comparison is displayed for several population time *T* (indicated top left) from the measured range.

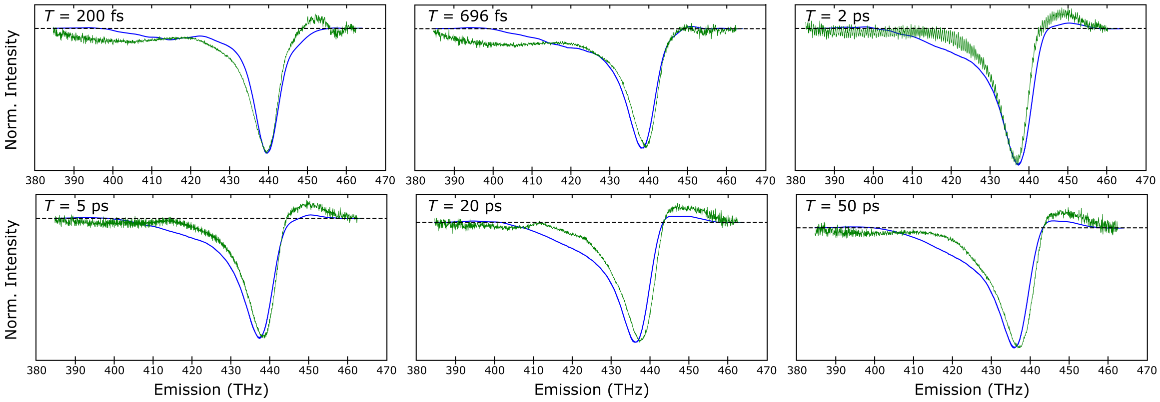

Figure S3. Phasing of the 2DES data of the N47H mutant at 77K. The phase is retrieved by means of the projection slice theorem, in which the projection of the real signal of the 2DES spectrum (blue) is compared to the measured pump-probe data (green).[1] The comparison is displayed for several population time *T* (indicated top left) from the measured range.

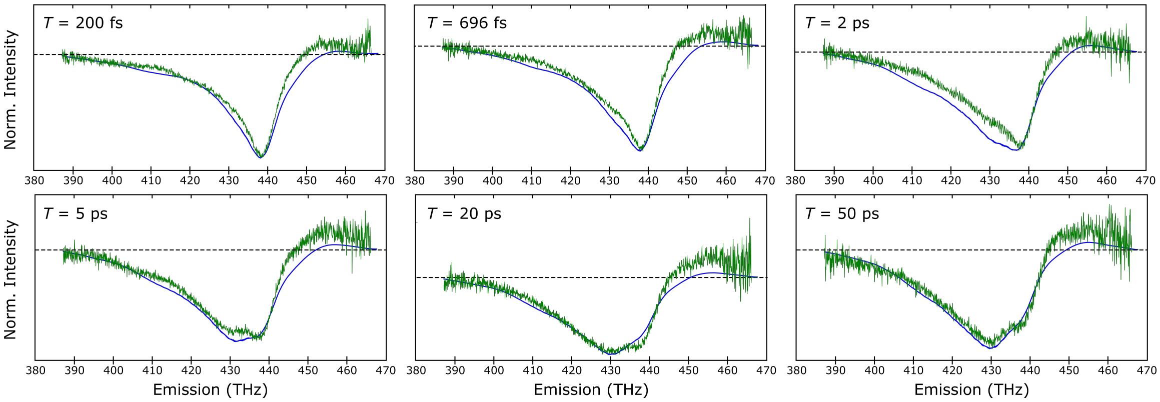

Figure S4. Phasing of the 2DES data of WT Lhca4 at RT. The phase is retrieved by means of the projection slice theorem, in which the projection of the real signal of the 2DES spectrum (blue) is compared to the measured pump-probe data (green).[1] The comparison is displayed for several population time *T* (indicated top left) from the measured range.

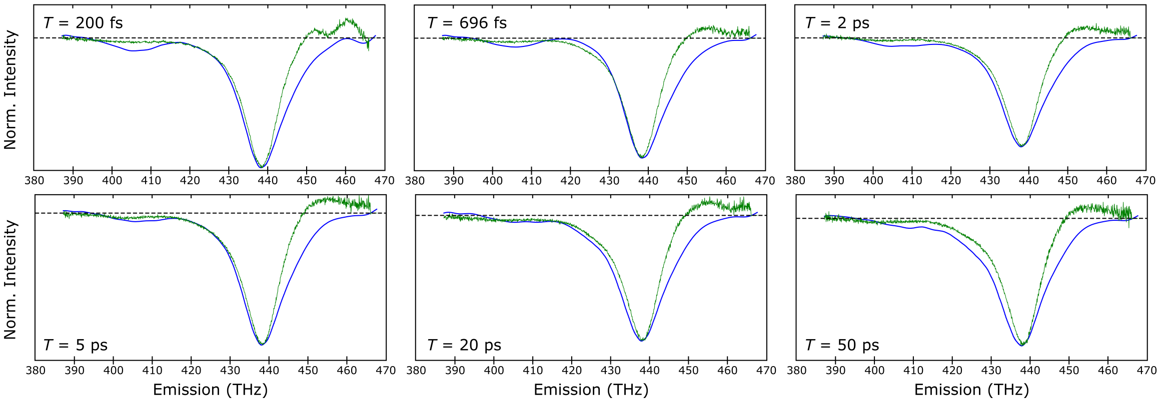

Figure S5. Phasing of the 2DES data of WT Lhca4 at 77K. The phase is retrieved by means of the projection slice theorem, in which the projection of the real signal of the 2DES spectrum (blue) is compared to the measured pump-probe data (green).[1] The comparison is displayed for several population time *T* (indicated top/bottom left) from the measured range.

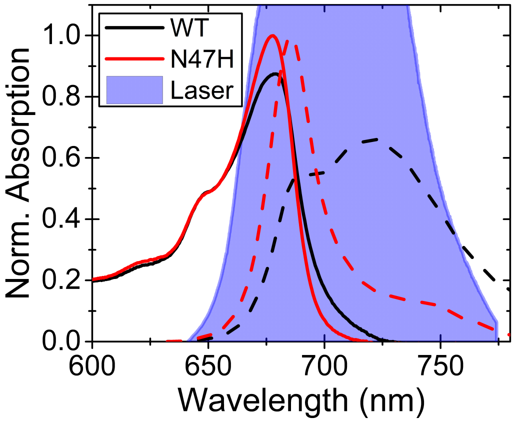

Figure S6. Steady-state absorption and fluorescence spectra of Lhca4 WT and N47H mutant at room temperature (RT). RT absorption (solid) and emission (dashed) spectra of Lhca4 WT (black) and mutant N47H (red). Emission spectra were recorded after excitation with 475 nm light. Absorption spectra are normalized to the area within the 600-780 nm region. The emission spectra are normalized to the absorption, and then scaled to one at the N47H fluorescence maximum to facilitate the visualization of the spectra. Spectrum of the laser pulses utilized in the 2DES experiments is shown in blue, and scaled with FWHM at 1 to indicate that the laser spectrum covers the red side of the major Chl *a* Q_y absorption band and the red forms region. The full laser spectrum is shown in Figure S1.

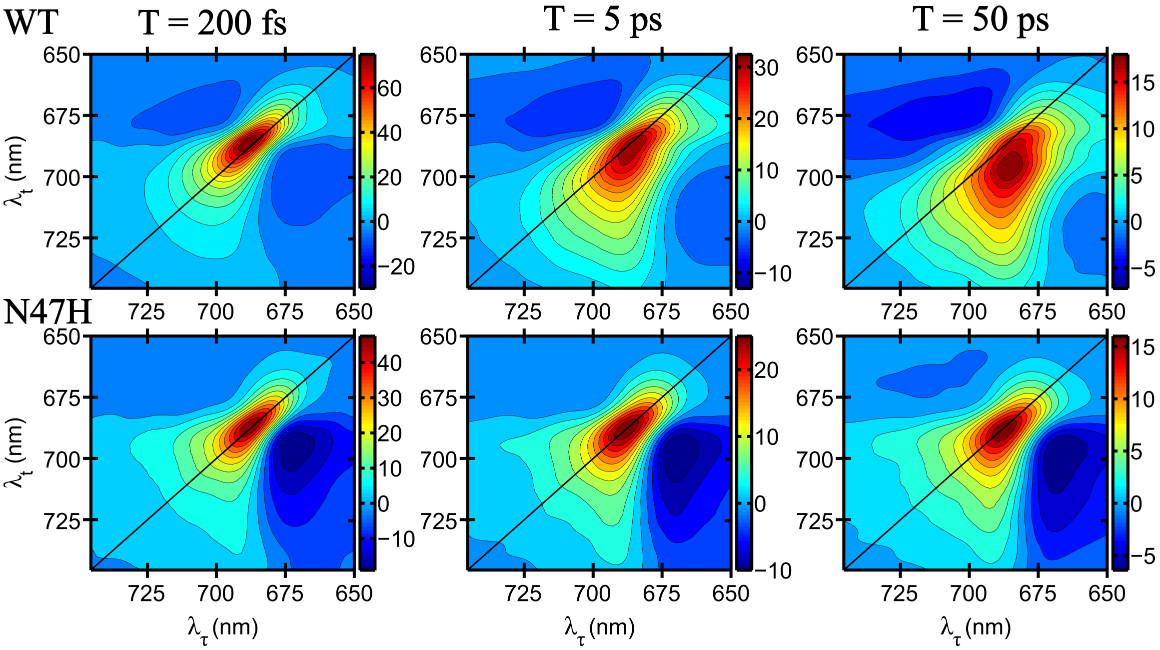

Figure S7. Real rephasing 2D spectra of Lhca4 at room temperature (RT). RT 2D spectra of WT (top) and N47H mutant (middle) Lhca4 at population times *T* = 200 fs, 5 ps and 50 ps.

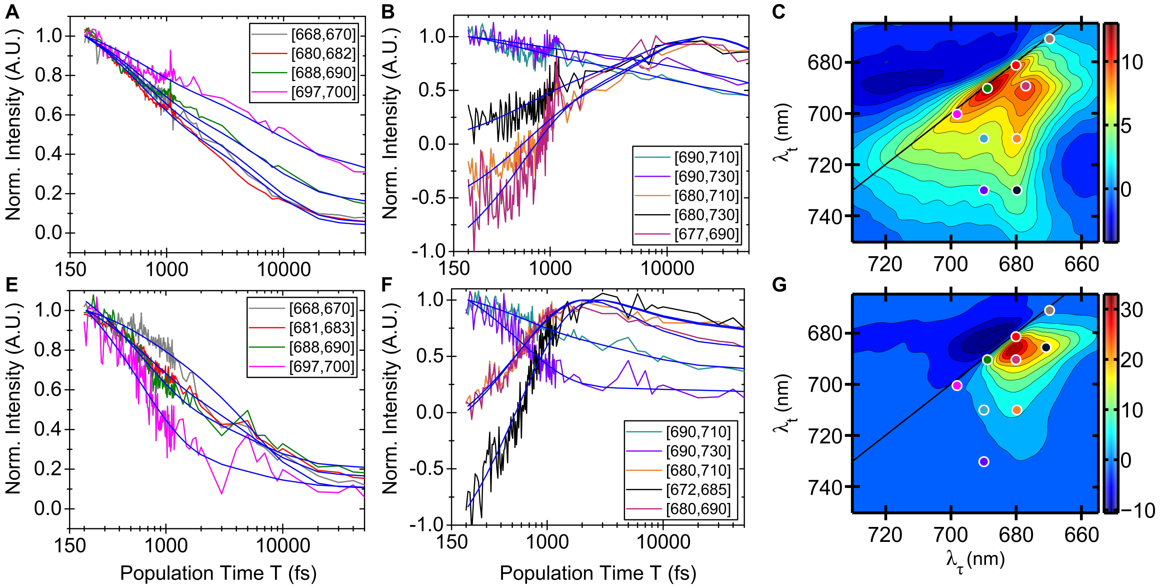

Figure S8. Global analysis fitting quality of Lhca4 2D spectral evolution. Transient kinetics of several diagonal (A and E) and anti-diagonal points (B and F) of the real rephasing 77K 2D spectra of WT (top, A and B) and N47H (top, B and F). Each curve is normalized to its maximum intensity to facilitate visualization of the traces. The position of the chosen points is indicated in the zoomed-in 50 ps 2D spectra of WT(C) and N47H (G). Dynamics of all curves is well captured with the exponential fit (blue curves) obtained from the global analysis of the entire 2D dataset.

Supplemental Methods

1. Exciton model of Lhca4

The model used in calculations is based on structural data of Qin et al.[2]. According to the data the Lhca4 complex contains 15 Chls when assembled as a hetero-dimer and associated with the PSI core. However, there is convincing evidence that the reconstituted complex used in our experiments, which is a monomer, does not contain some of the pigments, namely Chl 601, 617, and 618.[3] Therefore we use the 12-state model of reconstituted Lhca4, containing 9 Chls *a* (602-604, 609-614) and 3 Chls *b* (606-608). We also include a charge-transfer (CT) state corresponding to a charge separation between two Chls *a*, i.e. *a*603 and *a*609.

Exciton couplings have been calculated from the structural data in the point-dipole approximation supposing that the dipoles of the Chls Q_y transitions are directed from N_B to N_D atoms and the distance between the dipoles is equal to the distance between the Mg atoms of the two Chls. The effective transition dipole moments are supposed to be 4 and 3.4 Debye (D) for Chls *a* and *b*, respectively (as in our original model[3]). The transition dipoles, the center coordinates (corresponding to Mg atoms), and the center-to-center distances for all the 15 pigments of the Lhca4 complex are given in Tables S1 and S2. The couplings between the pigments are shown in Table S3.

Table S1. Transition dipole components dx, dy, dz (Debye) and center coordinates Rx, Ry, Rz (nm) for the pigments 601-618 of the Lhca4 complex. The z-axis corresponds to the normal to the membrane plane. The absolute values of the dipoles are 4 and 3.4 D for Chls *a* and *b*, respectively.

Pigment	dx	dy	dz	Rx	Ry	Rz
*a*601	3.1309	-2.4552	-0.4113	2.0032	1.7274	23.5366
*a*602	3.6497	-1.5714	-0.4587	3.2518	1.5771	23.8544
*a*603	-3.6678	-0.2202	-1.5807	4.1795	1.0559	23.3284
*a*604	0.0237	-2.2356	3.3169	4.8400	2.1828	21.9371
*b*606	-2.3285	-0.8765	2.3259	5.4467	1.6908	22.3123
*b*607	-2.4219	0.4931	2.3433	4.9184	0.9735	22.0316
*b*608	3.2035	0.4708	-1.0564	5.2382	2.2855	23.7886
*a*609	3.7923	-1.2006	0.4203	4.9901	1.2821	23.6276
*a*610	-3.6579	0.5006	-1.5392	4.2227	2.8237	23.5473
*a*611	-3.9042	0.8699	0.0148	2.4641	2.7486	23.1815
*a*612	3.5246	-0.5193	-1.8186	3.3461	2.8695	22.7491
*a*613	-0.1313	3.5834	1.7725	2.8323	1.3393	21.9802
*a*614	-1.5317	2.2223	-2.9522	2.1383	1.8741	21.6396
*a*617	-0.9825	-1.4111	-3.6116	5.7944	0.7188	23.9158
*b*618	1.9903	-2.3964	-1.3770	6.1482	2.9553	23.9606

Table S2. Distances between the transition dipoles (nm), calculated as distances between the Mg atoms of the pigments 601-618.

	*a*601	*a*602	*a*603	*a*604	*b*606	*b*607	*b*608	*a*609	*a*610	*a*611	*a*612	*a*613	*a*614	*a*617	*b*618
*a*601	0	1.297	2.287	3.288	3.654	3.366	3.292	3.021	2.475	1.175	1.930	1.805	1.907	3.941	4.343
*a*602	1.297	0	1.187	2.562	2.684	2.542	2.110	1.777	1.609	1.563	1.703	1.935	2.496	2.684	3.209
*a*603	2.287	1.187	0	1.908	1.743	1.494	1.686	0.893	1.781	2.414	2.078	1.926	2.772	1.751	2.807
*a*604	3.288	2.562	1.908	0	0.866	1.215	1.896	1.921	1.839	2.741	1.833	2.178	2.735	2.640	2.530
*b*606	3.654	2.684	1.743	0.866	0	0.934	1.605	1.451	2.075	3.281	2.448	2.658	3.381	1.907	2.192
*b*607	3.366	2.542	1.494	1.215	0.934	0	2.216	1.627	2.490	3.239	2.565	2.118	2.948	2.093	3.026
*b*608	3.292	2.110	1.686	1.896	1.605	2.216	0	1.046	1.174	2.877	2.236	3.155	3.794	1.667	1.142
*a*609	3.021	1.777	0.893	1.921	1.451	1.627	1.046	0	1.723	2.954	2.448	2.715	3.526	1.023	2.062
*a*610	2.475	1.609	1.781	1.839	2.075	2.490	1.174	1.723	0	1.797	1.186	2.567	2.980	2.652	1.973
*a*611	1.175	1.563	2.414	2.741	3.281	3.239	2.877	2.954	1.797	0	0.989	1.888	1.802	3.968	3.771
*a*612	1.930	1.703	2.078	1.833	2.448	2.565	2.236	2.448	1.186	0.989	0	1.787	1.918	3.461	3.054
*a*613	1.805	1.935	1.926	2.178	2.658	2.118	3.155	2.715	2.567	1.888	1.787	0	0.940	3.592	4.186
*a*614	1.907	2.496	2.772	2.735	3.381	2.948	3.794	3.526	2.980	1.802	1.918	0.940	0	4.459	4.757
*a*617	3.941	2.684	1.751	2.640	1.907	2.093	1.667	1.023	2.652	3.968	3.461	3.592	4.459	0	2.264
*b*618	4.343	3.209	2.807	2.530	2.192	3.026	1.142	2.062	1.973	3.771	3.054	4.186	4.757	2.264	0

Table S3. Couplings (cm^{-1}) between the pigments 601-618, calculated in the point-dipole approximation.

	*a*601	*a*602	*a*603	*a*604	*b*606	*b*607	*b*608	*a*609	*a*610	*a*611	*a*612	*a*613	*a*614	*a*617	*b*618
*a*601	0	-43.71	11.18	2.67	2.23	3.16	-2.19	-4.77	1.24	-50.36	3.73	5.55	-9.46	0.98	0.32
*a*602	-43.71	0	33.03	6.65	6.02	6.36	-8.96	-26.44	-10.32	8.52	16.91	-5.50	2.37	1.81	0.92
*a*603	11.18	33.03	0	-5.52	-12.72	1.31	8.16	171.41	14.34	-4.21	-1.64	2.59	-6.83	-11.10	-2.17
*a*604	2.67	6.65	-5.52	0	82.60	28.32	-1.00	-7.44	-5.39	-3.17	1.90	0.59	-3.49	4.58	1.75
*b*606	2.23	6.02	-12.72	82.60	0	59.16	-3.20	-3.97	-3.30	-2.82	3.27	1.31	-2.21	7.23	-1.47
*b*607	3.16	6.36	1.31	28.32	59.16	0	-4.39	-13.13	0.69	-3.02	2.95	0.60	-3.57	2.23	-0.93
*b*608	-2.19	-8.96	8.16	-1.00	-3.20	-4.39	0	51.74	50.35	4.35	-0.59	-1.99	1.47	-1.28	23.39
*a*609	-4.77	-26.44	171.41	-7.44	-3.97	-13.13	51.74	0	2.76	5.53	-2.80	-3.25	2.84	37.08	7.89
*a*610	1.24	-10.32	14.34	-5.39	-3.30	0.69	50.35	2.76	0	-25.37	16.43	7.12	-2.21	2.36	7.17
*a*611	-50.36	8.52	-4.21	-3.17	-2.82	-3.02	4.35	5.53	-25.37	0	130.33	-9.49	5.57	-0.48	0.69
*a*612	3.73	16.91	-1.64	1.90	3.27	2.95	-0.59	-2.80	16.43	130.33	0	-2.75	2.07	1.30	0.29
*a*613	5.55	-5.50	2.59	0.59	1.31	0.60	-1.99	-3.25	7.12	-9.49	-2.75	0	-76.54	-1.04	-0.77
*a*614	-9.46	2.37	-6.83	-3.49	-2.21	-3.57	1.47	2.84	-2.21	5.57	2.07	-76.54	0	-0.78	0.05
*a*617	0.98	1.81	-11.10	4.58	7.23	2.23	-1.28	37.08	2.36	-0.48	1.30	-1.04	- 0.78	0	-1.61
*b*618	0.32	0.92	-2.17	1.75	-1.47	-0.93	23.39	7.89	7.17	0.69	0.29	-0.77	0.05	-1.61	0

Coupling of the *a*603 and *a*609 sites to CT is 150 cm^{-1}, as was estimated from the fit of the spectra.[3] The diabatic CT state (i.e. the CT state in the absence of coupling to the excited states) is supposed to be dipole forbidden.

We use the unperturbed site energies of the 12 pigments and the CT state that have been extracted from the fit of the spectra (i.e. corresponding to the E2 set from Novoderezhkin et al.[3]). They are shown in Table S4. Diagonalization of Hamiltonian with the site energies from Table S4 and off-diagonal couplings from Table S3 gives us the energies and wavefunctions of the exciton states.

Coupling to slow conformations of the complex is accounted for using the model of static disorder, implying uncorrelated random shifts of the site energies described by a Gaussian distribution with a width of σ (FWHM). The disorder values for the Chls *a*, Chls *b*, and CT states determined from the fit are σ = 96, 67, and 144 cm^{-1} for Chls *a*, Chls *b*, and CT states, respectively.

Table S4. The site energies of the WT monomeric Lhca4 complex. The energies (in cm^{-1}) correspond to the pure electronic transitions without including a reorganization shift. The model includes 12 pigments from 15 obtained in the structure (i.e. *a*601, *a*617, and *b*618 are not included). The CT state corresponds to a charge transfer between the *a*603 and *a*609 pigments.

Site No.	1	2	3	4	5	6	7	8	9	10	11	12	-	-	13	
Pigment	601	602	603	604	606	607	608	609	610	611	612	613	614	617	618	CT
Chl*a*/*b*	*a*	*a*	*a*	*a*	*b*	*b*	*b*	*a*	*a*	*a*	*a*	*a*	*a*	*a*	*b*	
E2	-	15205	15039	15453	15856	15793	15731	15232	15345	15223	15190	15068	15190	-	-	14879

2. Compartmentalization and Redfield-Förster energy transfers

To model the excitation dynamics we use the combined Redfield-Förster theory. In this approach the whole Lhca4 reconstituted complex (with 12 pigments and one CT state) is split into 9 compartments, i.e. 4 strongly coupled dimers (602-603, 604-606, 611-612, and 613-614), and 5 monomeric states (607, 608, 609, 610, and CT). Then the dynamics within the strongly coupled clusters is described with the coherent modified Redfield theory, whereas the transfers between these clusters (with weak inter-cluster couplings) are treated with the generalized Förster theory. Recently we demonstrated that such a Redfield-Förster model of Lhca4 (denoted as cmRgF-9) gives the kinetics that are not much different from the exact hierarchical equations (HEOM) solution.[4]

The coherent modified Redfield (cmR) approach[5,6] is a non-Markovian secular master equation describing the dynamics of the one-exciton populations ρ_{ss} and the decay of the coherences $\rho_{ss'}$ between the exciton states. Non-secular terms, i.e. transfers between coherences and transfers between populations and coherences are not included. As in the original modified Redfield model[7] the diagonal exciton-phonon coupling is included explicitly, whereas the off-diagonal phonon-induced fluctuations (inducing relaxation between the exciton states) are treated perturbatively. The exciton wavefunctions are calculated by diagonalization of the pure exciton Hamiltonian, i.e. they are independent of the phonon coordinates, so that the dynamic localization is not included. In the Markovian limit (used in our study) the $s' \to s$ population transfers are given by the tensor $R_{s's'ss}$ that is the same as in original modified Redfield theory[7]:

$$
\begin{aligned}
& R_{sss's'} = 2\,\mathrm{Re}\int_0^{\infty} dt\, A_s(t)\, F^*_{s'}(t)\, V_{ss'}(t) \\
& A_s(t) = \exp\{i(\omega-\omega_s)t - g_{ssss}(t)\} \\
& F_s(t) = \exp\{i(\omega-\omega_s)t + 2i\lambda_{ssss}t - g^*_{ssss}(t)\} \\
& V_{ss'}(t) = \exp(2g_{s's'ss}(t) + 2i\lambda_{s's'ss}t) \times \\
& \times\big[\, \ddot{g}_{ss's's}(t) - \{\dot{g}_{s'ss's'}(t) - \dot{g}_{s'sss}(t) + 2i\lambda_{s'ss's'}\} \times \\
& \qquad \times \{\dot{g}_{s's'ss'}(t) - \dot{g}_{ssss'}(t) + 2i\lambda_{s's'ss'}\}\,\big]
\end{aligned}
\tag{S.1}
$$

where F(t) and A(t) are line-shape functions corresponding to fluorescence of the donor state and absorption of the acceptor, respectively, while V describes the interaction between donor and acceptor, ω_s is the energy of the s-th exciton state. Eq. (S.1) is valid for arbitrary delocalization of the donor and acceptor states. Other quantities are related to the exciton-phonon spectral density in the site representation $C_j(\omega)$:

$$g_{ss's''s'''}(t) = \sum_j c_j^s c_j^{s'} c_j^{s''} c_j^{s'''} g_j(t)$$

$$\lambda_{ss's''s'''}(t) = \sum_j c_j^s c_j^{s'} c_j^{s''} c_j^{s'''} \lambda_j$$

$$g_j(t) = -\int_{-\infty}^{\infty} \frac{d\omega}{2\pi\omega^2} C_j(\omega) \left[(\cos\omega t - 1) \coth\tfrac{\omega}{2\theta} - i(\sin\omega t - \omega t) \right] \tag{S.2}$$

$$\lambda_j = \int_{-\infty}^{\infty} \frac{d\omega}{2\pi\omega} C_j(\omega)$$

where $g_j(t)$ and λ_j are line-broadening function and reorganization energy of the j-th diabatic state. Amplitudes c_j^s show participation of the j-th site to the s-th exciton state. If the donor and acceptor states are localized at the j-th and i-th sites (i.e. $c_j^{s'}=1$ and $c_i^s=1$) then the transfer between them is given by the Förster formula, that can be obtained from (S.1) by replacing the interaction term by

$$V_{ss'} = \left| M_{ij} \right|^2 \tag{S.3}$$

where M_{ij} is the interaction energy corresponding to a weak coupling between the localized sites i and j. Switching to the Fourier-transforms of F(t) and A(t) we can rewrite the integral in a form of donor-acceptor spectral overlap.[8] The standard Förster formula can be generalized to the case of energy transfer between two weakly connected clusters.[9,10] The rate of energy transfer from the s'-th exciton state of one cluster to the s-th state of the other cluster is given by (S.1) with the interaction term:

$$V_{ss'} = \left| \sum_{i,j} c_i^s \, M_{ij} \, c_j^{s'} \right|^2 \tag{S.4}$$

where i and j designate molecules belonging to different clusters. In this generalized Förster formula, the donor and acceptor states s' and s can have an arbitrary degree of delocalization (corresponding to arbitrarily strong excitonic interactions within each cluster), but the inter-cluster interactions M_{ij} are supposed to be weak.

The decay of the coherences within strongly coupled clusters is given by[6]:

$$R_{ss'ss'} = \tfrac{1}{2} R_{ssss} + \tfrac{1}{2} R_{s's's's'} + \Gamma_{ss'}; \quad \Gamma_{ss'}(t) = \sum_j \left[(c_j^s)^2 - (c_j^{s'})^2 \right]^2 (\dot{g}_j(t) + i\lambda_j) \tag{S.5}$$

where R_{ssss} is the inverse lifetime of the s-th exciton state (determined by the sum of the s→s' relaxation rates $R_{s's'ss}$), $\Gamma_{ss'}$ is pure dephasing. In the Markovian approximation the time-independent dephasing term is (bearing in mind that $\mathrm{Im}\{\dot{g}(\infty)\} = -\lambda$):

$$\Gamma_{ss'}(\infty) = \sum_j \left[(c_j^s)^2 - (c_j^{s'})^2 \right]^2 \mathrm{Re}\{\dot{g}_j(\infty)\} \tag{S.6}$$

3. Exciton-phonon spectral density

To construct the exciton-phonon spectral density $C_j(\omega)$ (appearing in Eq. (S.2)) we use the Brownian oscillator model that includes the low-frequency overdamped part and underdamped terms reflecting a coupling to the high-frequency vibrations:

$$C_j(\omega) = 2\lambda_0 \frac{\omega\gamma_0}{\omega^2 + \gamma_0^2} + \sum_m 2\lambda_m \omega_m^2 \frac{\omega\gamma_m}{(\omega_m^2 - \omega^2)^2 + \omega^2\gamma_m^2} \quad ; \quad \lambda_m = S_m\omega_m$$

$$\lambda_j = \int_{-\infty}^{\infty} \frac{d\omega}{2\pi\omega} C_j(\omega) = \lambda_0 + \sum_m \lambda_m \tag{S.7}$$

where λ_0 and γ_0 denote coupling and characteristic frequency of an overdamped part of the Brownian oscillator, ω_m, S_m, λ_m and γ_m are frequency, Huang-Rhys factor, coupling and damping constant for the m-th vibrational mode.

Spectral density in a form of Eq. (S.7) with 48 high-frequency vibrations was used in our modeling of light-harvesting complex II (LHCII).[11] In the present modeling of Lhca4 we have taken the same spectral density with some adjustment of the damping constant γ_0 and coupling strength λ_0 for the overdamped part together with adjustment of the total Huang-Rhys S factor for the 48 high-frequency vibrations (the S factor has been adjusted by uniform scaling of all the couplings to vibrations λ_m, where m = 1-48). For Chls *a* the thus adjusted values are: $\gamma_0 = 40\ \mathrm{cm}^{-1}$, $\lambda_0 = 200\ \mathrm{cm}^{-1}$, S = 0.84. Following original Lhca4 model we suppose that the shape of the electron-phonon spectral density is the same for Chls *a*, Chls *b*, and CT, but the couplings (λ_0, λ_m) are different, i.e. the λ_0 and λ_m values determined for Chls *a* should be multiplied by 0.8, and 3.2 for Chls *b*, and CT, respectively.

Finally we note that the kinetics (and nonlinear spectral responses) calculated using Eqs. (S.1)-(S.7) should be averaged over realizations of the static disorder.

References

1 T. Brixner, T. Mancal, I. V Stiopkin and G. R. Fleming, Phase-stabilized two-dimensional electronic spectroscopy., *J. Chem. Phys.*, 2004, **121**, 4221–4236.

2 X. Qin, M. Suga, T. Kuang and J. R. Shen, Structural basis for energy transfer pathways in the plant PSI-LHCI supercomplex, *Science*, 2015, **348**, 989–995.

3 V. I. Novoderezhkin, R. Croce, M. Wahadoszamen, I. Polukhina, E. Romero and R. Van Grondelle, Mixing of exciton and charge-transfer states in light-harvesting complex Lhca4, *Phys. Chem. Chem. Phys.*, 2016, **18**, 19368–19377.

4 V. I. Novoderezhkin, R. Croce and R. van Grondelle, Dynamics of the mixed exciton and charge-transfer states in light-harvesting complex Lhca4: Hierarchical equation approach, *Biochim. Biophys. Acta - Bioenerg.*, 2018, **1859**, 655–665.

5 Y. H. Hwang-Fu, W. Chen and Y. C. Cheng, A coherent modified Redfield theory for excitation energy transfer in molecular aggregates, *Chem. Phys.*, 2015, **447**, 46–53.

6 Y. Chang and Y.-C. Cheng, On the accuracy of coherent modified Redfield theory in simulating excitation energy transfer dynamics, *J. Chem. Phys.*, 2015, **142**, 034109.

7 W. M. Zhang, T. Meier, V. Chernyak and S. Mukamel, Exciton-migration and three-pulse femtosecond optical spectroscopies of photosynthetic antenna complexes, *J. Chem. Phys.*, 1998, **108**, 7763–7774.

8 T. Förster, in *Modern Quantum Chemistry: Istanbul Lectures. Part III. Action of Light and Organic Crystals*, ed. O. Sinanoglu, Academic Press, New York, 1965, pp. 93–137.

9 M. Yang, A. Damjanović, H. M. Vaswani and G. R. Fleming, Energy transfer in Photosystem I of cyanobacteria *Synechococcus elongatus*: Model study with structure-based semi-empirical

Hamiltonian and experimental spectral density, *Biophys. J.*, 2003, **85**, 140–158.
10 V. I. Novoderezhkin and R. van Grondelle, Physical origins and models of energy transfer in photosynthetic light-harvesting, *Phys. Chem. Chem. Phys.*, 2010, **12**, 7352.
11 V. I. Novoderezhkin, M. a. Palacios, H. Van Amerongen and R. Van Grondelle, Energy-transfer dynamics in the LHCII complex of higher plants: Modified Redfield approach, *J. Phys. Chem. B*, 2004, **108**, 10363–10375.